Utilization of outer-midplane collector probes with isotopically enriched tungsten tracer particles for impurity transport studies in the scrape-off layer of DIII-D [a)]

D. C. Donovan,[1,b)] E. A. Unterberg,[2] P. C. Stangeby,[3] S. Zamperini,[1]
J. D. Auxier II,[1] D. L. Rudakov,[4] W. R. Wampler,[5] M. Zach,[2]
T. Abrams,[6] J. D. Duran,[1] J. D. Elder,[3] and A. Neff[2,c)]

[1]*Department of Nuclear Engineering, University of Tennessee-Knoxville, Knoxville, TN, 37916, USA*
[2]*Oak Ridge National Laboratory, Oak Ridge, TN, 37831, USA*
[3]*Institute for Aerospace Studies, University of Toronto, North York, ON M3H 5T6, Canada*
[4]*Center for Energy Research, University of California-San Diego, San Diego, CA, 92093, USA*
[5]*Sandia National Laboratory, Albuquerque, NM, 87123, USA*
[6]*General Atomics, 3483 Dunhill Street, San Diego, CA, 92121, USA*

(Presented XXXXX; received XXXXX; accepted XXXXX; published online XXXXX)
(Dates appearing here are provided by the Editorial Office)

Abstract (Limit 250 words): Triplet sets of replaceable graphite rod collector probes (CPs), each with collection surfaces on opposing faces and oriented normal to the magnetic field, were inserted at the outboard mid-plane of DIII-D to study divertor tungsten (W) transport in the Scrape-Off Layer (SOL). Each CP collects particles along field lines with different parallel sampling lengths (determined by the rod diameters and SOL transport) giving radial profiles from the main wall inward to $R\text{-}R_{sep}$~6cm. The CPs were deployed in a first-of-a-kind experiment using two toroidal rings of distinguishable isotopically-enriched, W-coated divertor tiles installed at 2 poloidal locations in the outer divertor. Post mortem Rutherford Backscatter Spectrometry of the surface of the CPs provided areal density profiles of elemental W coverage. Higher W content was measured on the probe side facing along the field lines toward the inner divertor indicating higher concentration of W in the plasma upstream of the CP, even though the W-coated rings were in the outer divertor. Inductively coupled plasma mass spectroscopy validates the isotopic tracer technique through analysis of CPs exposed during L-mode discharges with the outer strike point on the isotopically-enriched W coated-tile ring. The contribution from each divertor source of W to the deposition profiles found on the mid-plane collector probes was able to be de-convoluted using a Stable Isotope Mixing Model. Results provided quantitative information on the W source and transport from specific poloidal locations within the lower outer divertor region.

I. Introduction

The use of solid, electrically-floating objects, with dimensions ~ 1cm, inserted into the edge of tokamaks to measure deposition (or 'collection') of impurity ions in this region has been used in magnetic fusion energy (MFE) research for decades[1-4]. These objects, termed collector probes (CP) here, are used to study impurity production and transport from plasma-facing components (PFCs) in the SOL (scrape-off layer) of magnetically confined fusion energy (MFE) devices[5-9].

In this work, we examine the function and analysis of the impurity collector probe diagnostic focusing on three primary aspects. The deposited material used is tungsten (W) for reasons given later. The first aspect, described in Section II.C, defines the CP sampling length which has 3 different values for the 3 different probe sizes, from ~cm to ~m scale lengths along the magnetic field lines; such spatial resolution greatly aids understanding of SOL impurity transport. The second aspect, described in Section III.A, relates to the interpretation of the RBS-measured deposition profiles on the upstream and downstream facing-sides of each probe – namely the relative magnitudes and the radial decay lengths - from which can be inferred basic features about parallel and perpendicular impurity transport in the SOL. The third aspect, described in Section III.B, is how the combined use of CPs and isotopic W tracer particles makes it possible to relate the specific source location of the W in the divertor to the transport of the W in the SOL; this makes the combination of CPs with isotopic W tracer particles a global, rather than just a local, impurity transport diagnostic for the boundary plasma.

II. Experimental Setup

A. DIII-D Metal Rings Campaign

The implementation of the midplane collector probes and isotopically enriched W tracer particles described in this

[a)] Published as part of the Proceedings of the 22nd Topical Conference on High-Temperature Plasma Diagnostics (HTPD 2018) in San Diego, California, USA.
[b)] Author to whom correspondence should be addressed: ddonovan@utk.edu.
[c)] Oak Ridge Institute for Science and Education (ORISE) Postdoctoral Fellow.

work was part of the DIII-D Metal Rings Campaign (MRC) of June 2016 [10, 11]. The experimental setup used in DIII-D was similar to the one in ASDEX-Upgrade (AUG) [5, 6, 12-14], although AUG used natural (not isotopically-enriched) W and employed a single deposition cylinder rather than a triplet set. On DIII-D, the setup involved the installation of a full toroidal array (ring) of molybdenum inserts coated with natural W on the lower, horizontal divertor floor (natural W is 26.5% W-182) and another full toroidal array coated with 93% enriched W-182 on the horizontal divertor shelf. The location of these two divertor metal rings and the midplane collector probe can be seen in Figure *1*, which shows the poloidal cross-section of the DIII-D vessel and the position of this setup as related to a typical DIII-D discharge.

B. Collector Probe Design

A triplet set of graphite collector probes was mounted within a holder on the DIII-D midplane retrofit to a moveable insertion arm usually used for Langmuir probe (LP) measurements[15, 16]. The drive mechanism of this arm allows for probe-dwell at a specified insertion depth into the edge plasma near the outboard mid-plane and with the capability to retract the probes after exposure behind a gate valve into a separately pumped cavity. This allowed probes to be removed between shots and replaced with clean probes without affecting the primary vacuum of the vessel. This made it possible to expose a large number of probes throughout the campaign, covering a wide range of plasma conditions. The arm inserts almost precisely radially (R in Figure *1*). The vertical axis of the device is denoted by Z in Figure *1* and the elevation of the centerline of the arm assembly is at Z = -18.5 cm, i.e. below the device mid-plane (Z = 0 cm). There is a slight radial offset due to the insertion angle (~13°) of the arm, which is taken into account when converting the radial length along the probe to radial distance from the separatrix ($R - R_{sep}$) (separatrix can be seen in Figure *1*) for each face of each collector probe. This offset amounts to a <2.5mm difference in the individual CP and plasma coordinates. Each probe in the triplet set, shown in Figure *2* mounted in the holder, has a different diameter in order to measure the W content of the plasma over different parallel sampling lengths along the SOL (smaller diameter corresponds to shorter sampling lengths, described in detail in the next section). The three probes making up the triplet set are labeled Type A, B and C. Types B and C probes were both machined from ATJ graphite (the same graphite used to make the DIII-D wall tiles) into cylindrical rods with lengths of 11.75 cm. Type B (C) probes have a 1 (0.5) cm diameter. Two flat surfaces were machined on opposite sides along the axis of the rods in order that the sampling surfaces be normal to the direction of the magnetic field. Type A probes consisted of two 0.635 cm (1/4 inch) diameter graphite cylinders (made from Ted Pella, Inc. Spectroscopically Pure Carbon[17]) that were inserted inside a 3 cm diameter hollow graphite cylinder, as shown in Figure *3*. The Type A probe housing was re-used for each shot

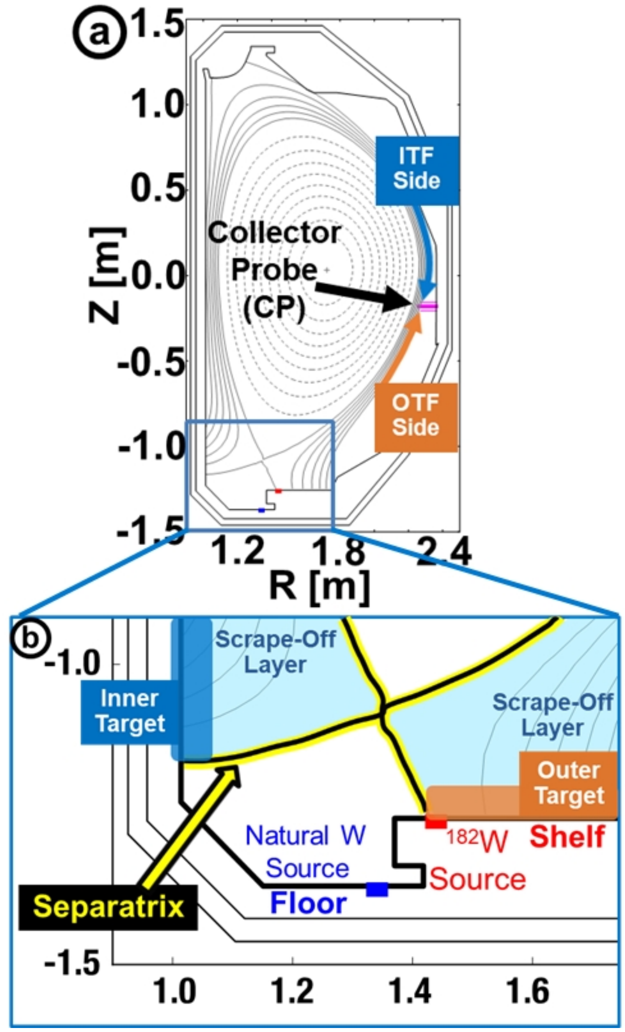

Figure 1: Magnetic flux surface configuration for DIII-D L-mode discharge 167196. a) Full poloidal cross-section of DIII-D. CPs are oriented normal to the magnetic field lines and collect on opposing sides. b) Locations of the toroidal array of tiles coated in natural W on the divertor floor and the enriched W-182 toroidal array on the divertor shelf.

while the two inserts were replaceable. Although the Type-A probe requires more interpretive effort (see Section III.A), it allows for an operationally simpler CP. During the campaign 37 pairs of Type-A inserts were exposed as well as 10 Type-B and Type-C CPs.

Knowing the geometrical setup of the CP within the DIII-D vessel and the pitch of the field-lines/flux tubes, it is possible to identify the locations of the sources of the deposited ions. The field pitch and helicity of the flux tube varies with the B-field configuration used during the CP exposure. To maintain consistency regardless of field direction, the term 'Inner Target Facing' (ITF) will be used here to refer to the 'upstream' side of the probe, which is the face that connects along field lines in the direction toward the inner target. 'Outer Target Facing' refers to the 'downstream' side of the probe, which connects along field

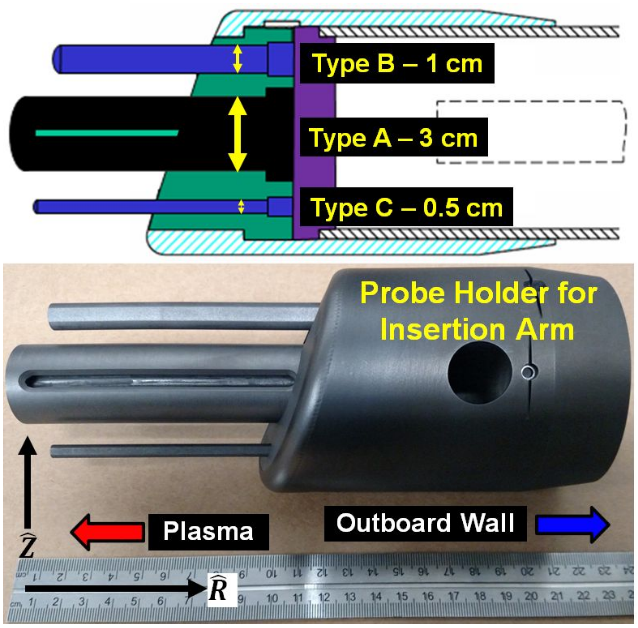

Figure 2: DIII-D triplet collector probe set mounted on mid-plane insertion arm holder ready for insertion into the far-SOL plasma. The diameter of each probe type is shown. The Type-A probes are inserted into a 3 cm diameter holder.

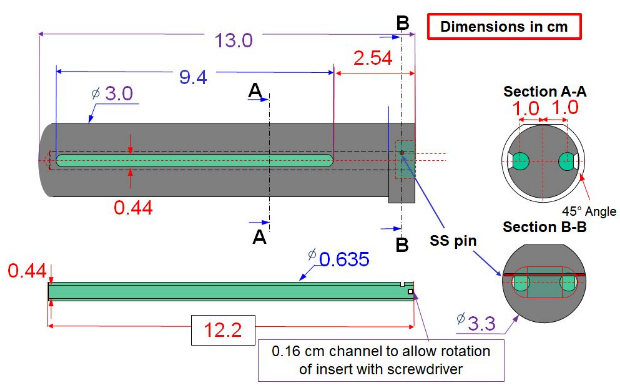

Figure 3: Schematic of Type A probe assembly. Top shows 3 cm diameter probe holder. Bottom shows insert that is slid into probe holder and held in place with a stainless steel (SS) pin. Two inserts are used for each exposure, both with only one flattened surface facing opposite directions and oriented normal to the direction of the magnetic field.

lines in the direction toward the outer target. The ITF and OTF naming convention is indicated in Figure *1*.

A standard definition of the *connection length* of a divertor tokamak is half the distance along field lines between divertor targets[18]. The *connection length of a CP* is taken here to be half the distance along field lines between the CP and the next solid surface encountered, which is either a divertor target or part of the main vessel wall. Thus the connection length of a CP is different for the two faces of the CP and it can also vary considerably with radial location along the axis of the CP since in the far SOL, the wall may be only a short distance from the CP along a field line. Because the CP in DIII-D is located near the outer-midplane, the CP connection length is always shorter for the OTF than the ITF – at least it is for the near SOL where the ITF connection length involves field lines that go up to the crown of the plasma and back down to the inner target. In the far SOL, the field lines can hit the main wall and therefore any 3D structures can affect the connection length.

It is necessary to distinguish between the *connection* length (L_{conn}) and the *collection* length (L_{coll}) of solid probes including CPs. If a CP is large enough then it acts as a main limiter, and in the simplest picture impurity ions diffuse cross-field into the flux tube subtended at the one end by the CP and at the other end by a divertor target or part of the main wall. Within that flux tube the ions then 'feel' the sink action of the two solid surfaces ~equally and travel along the field lines to those surfaces, half the ions being collected on the one solid surface, half on the other. Thus in this situation the CP measurement capabilities are limited by the *connection* length.

When a probe is small enough, however, the parallel sink action that it exerts only extends a distance along the field lines which can be shorter than its connection length, i.e. its *collection* length is shorter than its *connection* length. A simple expression for L_{coll} includes diffusive cross-field transport[17-19]:

$$\textit{Diffusive}: L_{coll} \sim d^2 c_s / 4D_\perp \qquad (1)$$

where d is the characteristic size of the probe, e.g. the diameter of a CP rod, $D_\perp$ is the cross-field diffusion coefficient, and the plasma sound speed $c_s \approx (2\,kT_e/m_i)^{1/2}$ with m_i the mass of deuterium. Eqn. (1) is adapted from Fig. 7 and eqn. (2.10) of [Ref 19], in which a square collecting surface was assumed rather than a cylinder as applies here. Eqn. (1) also describes the situation for a probe of any size, however large, in a plasma of infinite spatial extent. If the cross-field transport is assumed instead to be convective with velocity $v_\perp$, rather than diffusive, then eqn. (1) is replaced[20-22] by:

$$\textit{Convective}: L_{coll} \sim d c_s / v_\perp \qquad (2)$$

Thus the collection length of a CP depends on its size with small diameter CPs sampling the plasma impurity content just near the CP, and larger diameter ones collecting ions spanning over a greater distance from the CP, up to the connection length of the CP. The actual measurement length of a CP, henceforth distinguished by the name *sampling length* (L_s), is the smaller of its connection length and the collection length given by eqn. (1) or (2).

Because the collection length is proportional to c_s, it varies radially as $L_{coll} \propto T_e^{1/2}$. T_e falls off monotonically with R-R_{sep} and is measured in the boundary plasma region of DIII-D using both the Thomson scattering diagnostic and a mid-plane reciprocating Langmuir probe. A series of 25 repeated L-mode discharges (DIII-D discharges 167196-167220) during the MRC have been chosen for a more detailed analysis of the variation in the connection length as a function of distance along the probe. For these L-mode discharges discussed in this work, the SOL is approximated as existing in the diffusive cross-field transport regime, used to create eqn. (1). The conditions for these discharges were

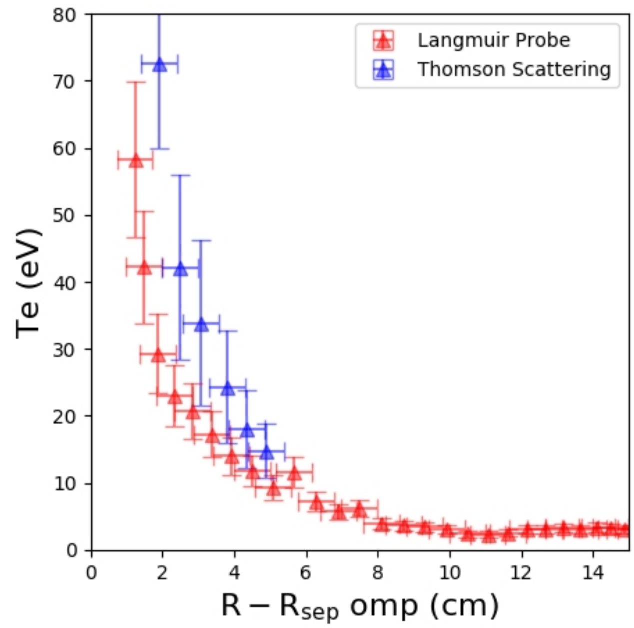

Figure 5: Electron temperature (T_e) profile of the far-SOL plasma obtained from repeated insertion of the plunging Langmuir probe located near the outer mid-plane and the DIII-D Core Thomson Scattering diagnostic.

1.2 MA plasma current, 2.1 T toroidal magnetic field, and 3.8 MW injected beam power.

The T_e profile of the SOL as measured by Thomson scattering and the mid-plane plunging Langmuir probe is shown in Figure 5 plotted with respect to R-R_{sep} mapped to the outer mid-plane (OMP). Temperature ranges from ~12 eV at the peak insertion depth of the collector probes (R-R_{sep} ≈ 6 cm) to ~3 eV at the outer end of the probe (R-R_{sep} ≈ 16 cm). Since T_e decreases as the distance from the separatrix increases, the collection length along the R-R_{sep} axis of the collector probe decreases. The combined profiles of L_{conn} (obtained from magnetic field line mapping for both the OTF and ITF directions) and L_{coll} (calculated using Eqn. (1) using T_e values from Figure 5) are shown in subfigure a) of Figure 4. L_{conn} is only plotted for the Type A probe, but the profiles for Types B and C are nearly identical up until R-R_{sep} ≈ 12 cm, with only minor differences between the probes beyond that point. Subfigure b) of Figure 4 shows the sampling length for both the OTF and ITF sides of the Types A, B, C probes. Because the sampling length (L_s) is the lesser of L_{conn} and L_{coll}, the L_s for the Type A probe is nearly always defined by L_{conn}. For the Type B probe, L_s is equal to L_{coll} up to R-R_{sep} ~ 11 cm for the ITF side. For the Type C probe, L_s is equal to the L_{coll} for the entire probe on both sides.

Through this calculation of the sampling lengths, 2D and 3D visualizations of the sampling lengths of the collector probes can be created, as shown in Figure 7 and Figure 6, respectively. The 2D poloidal cross-sections of DIII-D are shown with the sampling lengths parallel to the magnetic field lines for probe types A, B, and C projected onto the 2D plane. They demonstrate how the Type A probe

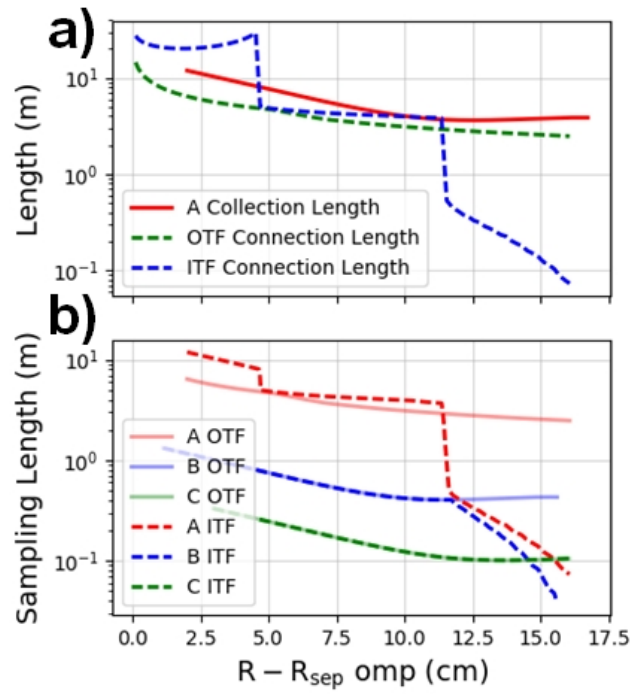

Figure 4: a) Only the collection and connection lengths for the Type A probe are shown for the L-mode discharges assuming diffusive cross-field transport. b) Sampling lengths are shown for the Type A, B, C probes for both the OTF and ITF sides for the L-mode discharges discussed.

is capable of sampling over a significantly larger poloidal range. Whereas the Types B and C probes are sampling very near to the poloidal location where the collector probe is inserted. As will be shown in the results, the ex-situ analysis of the deposits on the Type A probes did indeed exhibit different behavior than those measured on the Types B and C probes. The 2D poloidal cross-sections assume toroidal symmetry, but plotting the field lines in 3D allows for better assessment of where the field lines intercept a limiting object before reaching the inner or outer targets near the divertor. Limiting objects will act as sources and sinks of particles as impurities are deposited and re-eroded. Because these L-mode discharges were at the beginning of the campaign, no appreciable levels of re-deposited W had yet deposited on any surfaces. However, the longer the campaign continued, the more the W coating was gradually re-deposited throughout the device and particularly on limiting surfaces.

III. Ex-Situ Analysis of Collector Probes

A wide variety of parameters were studied during the various operating configurations of the DIII-D MRC including H-mode/L-mode, injected power, strike-point positioning, ELM frequency and deposited power. The collector probes were typically left in place for between 1 to 4 repeat plasma pulses and the penetration depth of the collector probes was varied during the campaign to obtain the optimal distance from the separatrix for collecting interpretable data. The results discussed in this paper focus on a triplet set of collector probes exposed for a series of 25

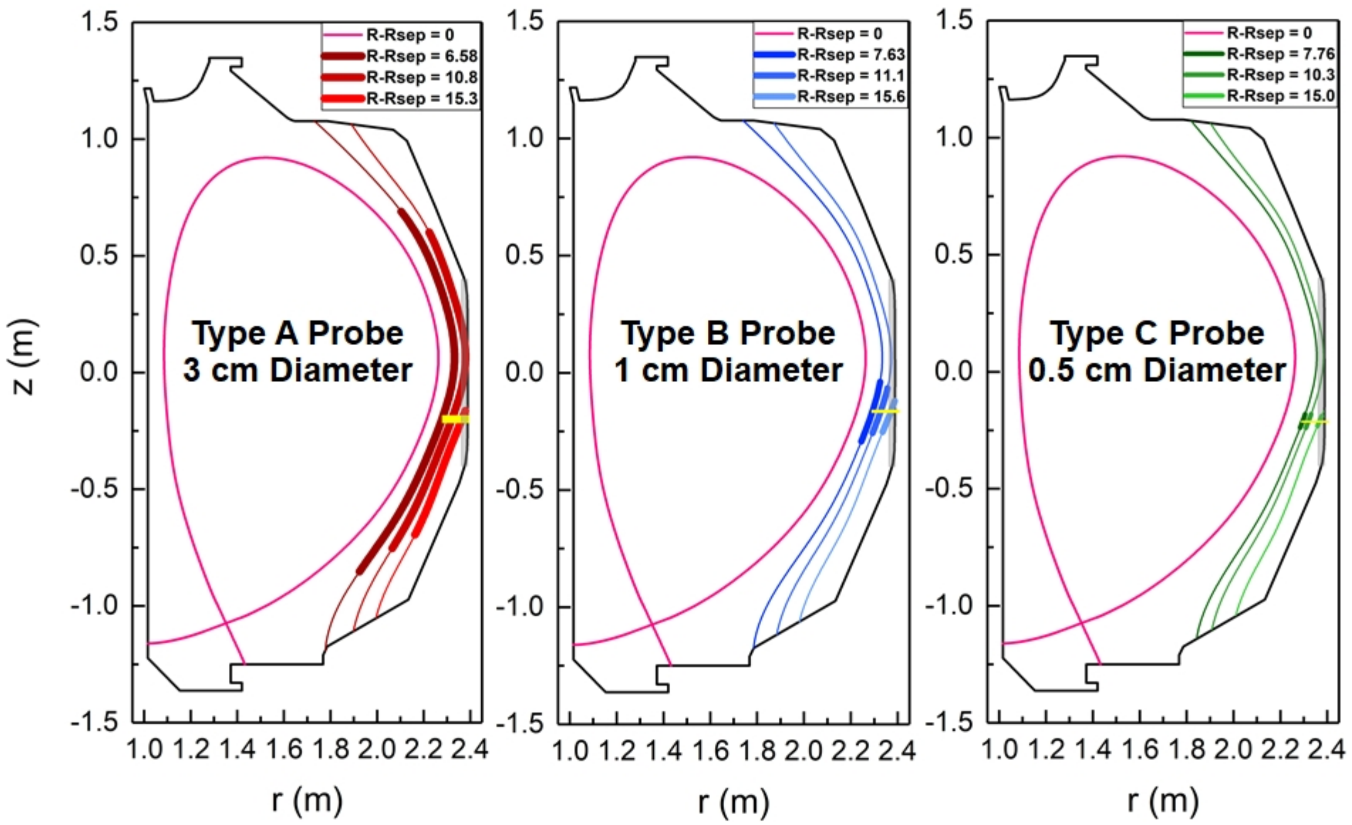

Figure 7: Sampling lengths (parallel to magnetic field lines) of collector probe types A, B, C are projected on a 2D poloidal cross-section for L-mode discharges discussed. The magenta line denotes the location of the last closed flux surface (LCFS). The thinner lines in the SOL represent the magnetic field lines that intercept the collector probes. The thicker lines represent the sampling length of the probe (in poloidal projection). Three lines are shown corresponding to three different $R\text{-}R_{sep}$ positions along the axis of each type of probe.

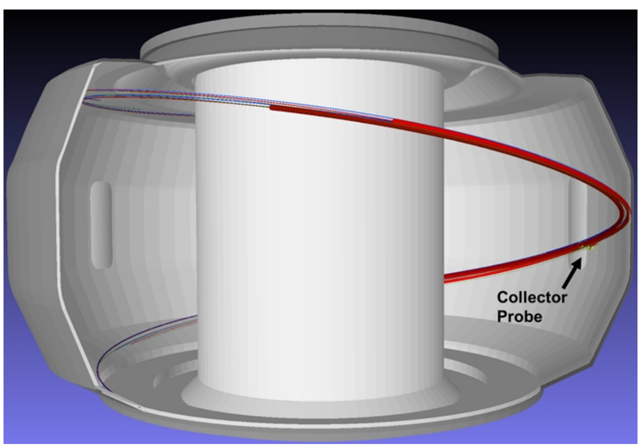

Figure 6: 3D plot of sampling lengths (thick lines) of the Type A probe. The thin lines are the magnetic field lines intercepting the probe that eventually reach the inner and outer targets. Two lines are shown corresponding to three different $R\text{-}R_{sep}$ positions along the length of the Type A probe.

repeat L-mode discharges that took place at the beginning of the MRC. The two primary types of *ex-situ* analyses were RBS and Inductively Coupled Plasma Mass Spectroscopy (ICP-MS).

A. Rutherford Backscatter Spectroscopy (RBS) Analysis

RBS is a non-destructive elemental analysis technique (cannot distinguish W isotopes) capable of providing highly accurate quantitative measurements of tungsten areal density, σ_W (W atoms/cm^2) on the surfaces of the collector probes with resolving capabilities down to ~10^{12} W atoms/cm^2. The measurements were performed at SNL using a monoenergetic 2 MeV He-4 analysis beam.[20, 21] The RBS measurements were made every 5 mm along the axis of the exposed region of the probe on both the OTF and ITF sides. RBS was also the primary ex-situ analysis technique used in previous collector probe campaigns on other devices (AUG[4], JET[22], T-10[23]) to measure impurity deposition profiles. These deposition profiles have been measured for a wide range of plasma conditions in the DIII-D MRC and some key similarities with previous uses of collector probes have been identified, along with some important new features discovered through the use of different diameter probes.

Analysis of the full set of CPs showed a wide range of peak σ_W, which usually occurs near the tip of the probe nearest the separatrix. Although all probes analyzed with RBS have shown measurable levels of W at some location on the probe, there were a number of conditions where the peak σ_W was very near the RBS threshold of ~1×10^{12} W atoms/cm^2, which left much of the rest of the W content along the remainder of the probe below the measurement

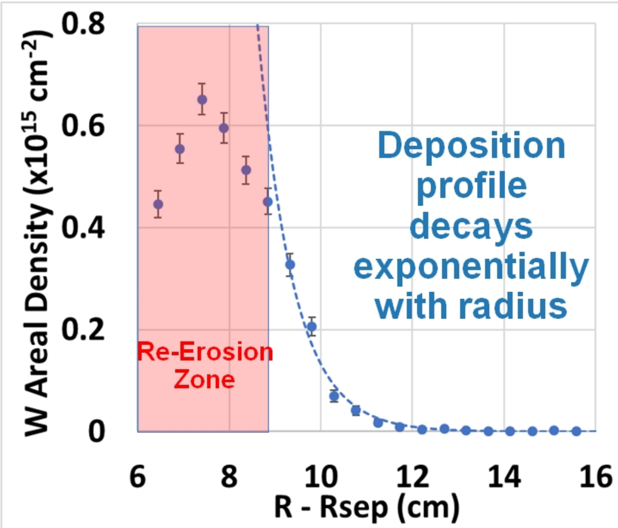

Figure 8: Deposition profile on a Type B probe exposed during L-mode discharges 167196-167220 as measured by RBS demonstrating a typical deposition profile seen on the collector probes with an exponentially decaying region defined by a radial decay length (λ) and a re-erosion zone near the exposed region at the tip closest to the separatrix.

threshold. However, a majority of the probes had enough deposited material to measure the content along nearly the entire length of the probe. The collector probes with some of the highest deposited content were those exposed during the set of 25 repeated L-mode shots that were described in the previous section.

The deposition profiles shown in Figure 8 and Figure 9 have several features that are representative of the majority of collector probes surveyed following the DIII-D MRC and that were observed on previous collector probe experiments[4, 24]. The W deposition profiles are well-fit as exponentially decaying radially. The exception is the region nearest to the inner ends of the probes where σ_W begins to plateau, and in some cases even decreases slightly, where the W deposits are being re-eroded. This "re-erosion zone" was observed on the collector probes of previous experiments as well, particularly on AUG[4], and is due to the parallel particle flux density of fuel and low-Z ions and T_e increasing as the collector probes penetrate closer to the separatrix, thereby increasing the sputtering and erosion rate of the deposited W. These features of the typical deposition profile are shown in Figure 8. The W deposition profiles as measured by RBS for the OTF and ITF sides of the Types A, B, and C probes exposed during Shots 167196-167220 are shown in Figure 9. The re-erosion zone gives an indication of the near- vs. far-SOL boundary where one could expect the physics assumptions of Eq. 1 to start to apply. The re-erosion is an indication that, the probe had been inserted to its maximum extent for this exposure condition for readily interpretable measurements.

When the remainder of the deposition profile beyond the re-erosion zone is fit with an exponential ($y(x) = y_0 e^{-x/\lambda}$), then the Radial Decay Lengths (RDL) can be determined for the profiles on the ITF (λ_{ITF}) and OTF (λ_{OTF})

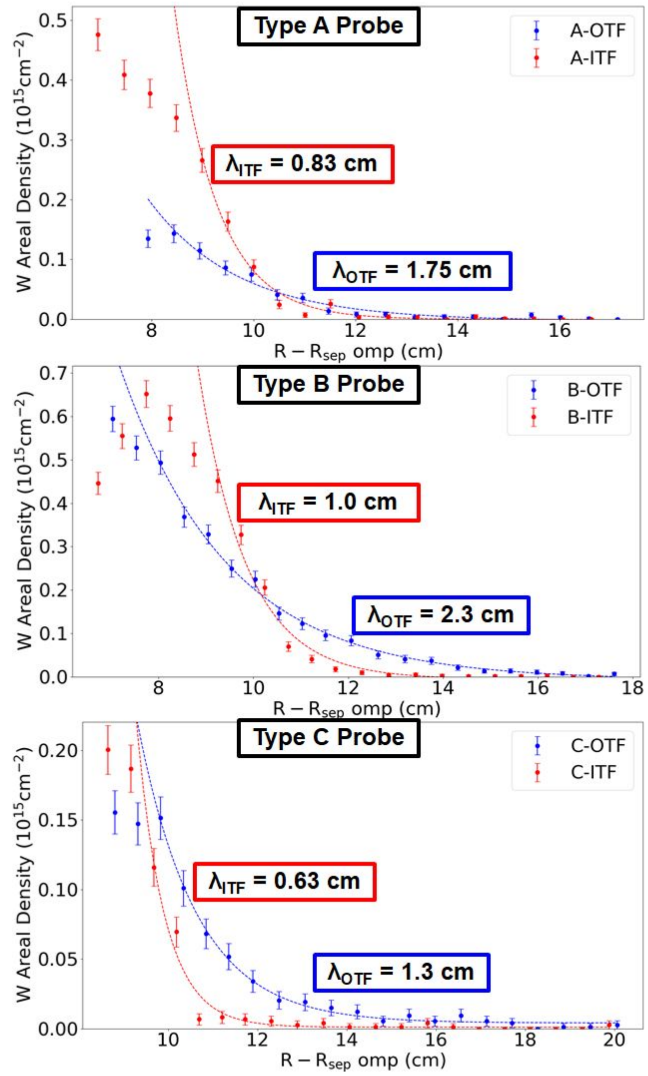

Figure 9: Deposition profiles as measured by RBS from the OTF and ITF sides of probes A, B, C from the repeated L-mode exposures (shots 167196-220). In each case, the deposition profiles decay radially, which can be fit to assess radial decay length (λ).

sides of each probe. Approximate expressions can be formulated for the RDL using similar assumptions used to create Eqns. 1 and 2. More detail on the interpretation of the RDL can be found in Ref. 18, 24, 2.

One of the key observations from these L-mode deposition profiles is that for probe type A, the ITF side was found to have a significantly higher peak σ_W (~5 x 10^{14} W/cm^2) than was found on the OTF side (~1.5 x 10^{14} W/cm^2). For the same shots, the Type-B CP had nearly the same peak σ_W on its ITF and OTF sides (~6 x 10^{14} W/cm^2). The Type-C probe also shows nearly the same peak σ_W on its ITF and OTF sides (~2 x 10^{14} W/cm^2). This difference between σ_W on the ITF and OTF sides can be clearly seen in *Figure 10*, which plots the ratio of the ITF side σ_W to the OTF side σ_W for the same R-R_{sep_omp} position as a function of the minimum sampling length (the lesser of the OTF and ITF sampling lengths at the same R-R_{sep_omp} location is used). Only measurements from outside of the "re-erosion

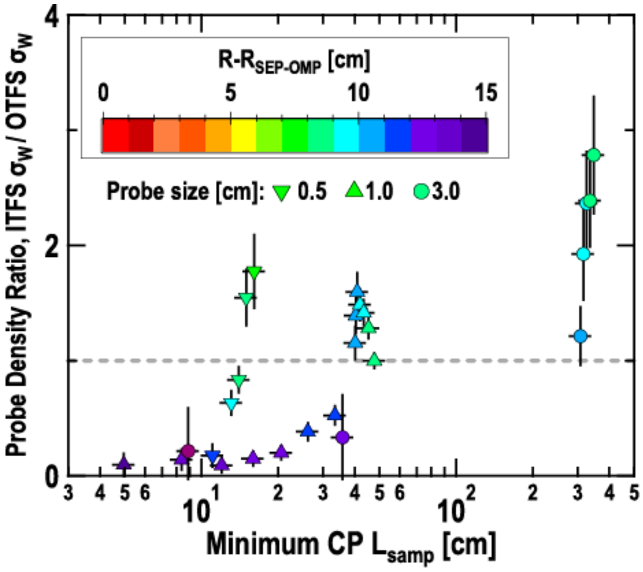

Figure 10: Ratio of W areal density measured on the ITF side to the OTF side of the CPs. Ratios are only obtained for points outside of the "re-erosion zone" on the CPs. Points are included from the Types A (3 cm), B (1 cm), C (0.5 cm) probes and are plotted as a function of the minimum CP sampling length of either the ITF or OTF side of the probe at the measurement location. The points are color-coordinated to indicate distance from the separatrix.

zone" (seen in Figure 8) are used. The figure highlights the fact that sampling lengths are longest closer to the separatrix and that the longest sampling lengths correspond to the largest ratios of ITF side σ_W to OTF side σ_W.

The type A probe has the longest sampling length (~4 m upstream and downstream, parallel to B) because it is the widest diameter probe (3 cm), whereas the types B and C probes are only sampling the region within <1 m upstream and downstream of the collector probe. This indicates that the type A probe is sampling a region of increased W density in the plasma in the direction of the inner target, which is beyond the reach of the types B and C probes. The sampling length of the type A probe is not long enough to reach all of the way to the inner target, but it is capable of reaching towards the crown of the tokamak, as seen in Figure 7. This is suggestive of a higher density of W impurities existing in that region of the plasma. An "impurity potential well" has been hypothesized to occur in the SOL between the targets and has arisen in DIVIMP modeling of carbon impurities in the plasma[25, 26]. The discussion of DIVIMP modeling of W transport in the DIII-D MRC is beyond the scope of this paper and will be detailed in a separate publication.

B. Measuring Isotopic Ratios on the Collector Probes

Using multiple isotopic sources of W in a fusion experiment, each with a unique "fingerprint" (i.e. relative fractions of stable isotopes W-180, W-182, W-183, W-184, W-186) created by artificially enriching one isotope more than the others, enables the use of isotopic tracers that can

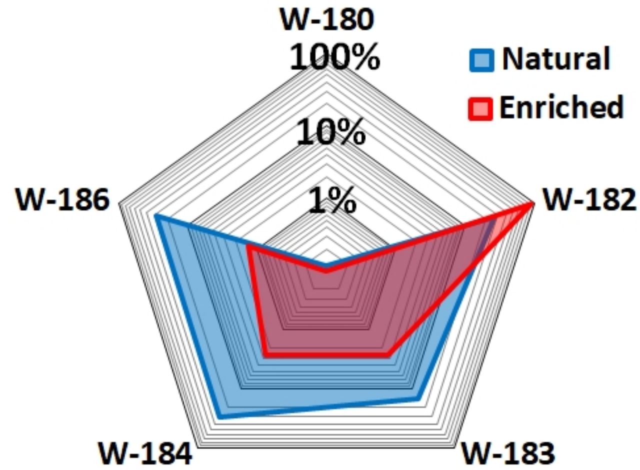

Figure 11: The isotopic fraction of each of the 5 stable isotopes of W (180, 182, 183, 184, 186) are shown for the 2 types of isotopic W used on DIII-D. (Blue) Natural W – 26.5% W-182; (Red) Enriched W – 93% W-182. When the two sources mix, they combine to form a new, unique 'isotopic fingerprint' that is deposited on the CP. The amount contributed from each source to make the unique result on the CP can be found using the Stable Isotope Mixing Model (SIMM).

be collected at other locations in the device. As each source of W on different toroidal rings of the device erode at different rates depending on the plasma condition and configuration, the particles are sputtered into the SOL plasma and mixed together. The mixture is a combination of the various sources, with the prevalence of each source weighted in the final mixture by the relative flux of impurities leaving each of their respective original sources. When the mixture deposits on a collector probe in another region of the device, a new unique isotopic fingerprint exists on the probe. The DIII-D MRC used natural W (26.5% W-182) and enriched W (93% W-182) at different locations on the divertor, as shown in Figure 1. These had distinct isotopic "fingerprints" as shown in Figure 11.

Isotopic analysis of the W deposited on the collector probes was performed using two different forms of ICP-MS. Inductively Coupled Plasma Time-of-Flight Mass Spectroscopy (ICP-TOF-MS)[27] provides high sensitivity (parts per trillion) analysis with the ability to rapidly scan a wide range of the mass spectrum using a quadrupole system. The analysis of the DIII-D MRC used a GBC Scientific Optimass 9500 ICP-TOF-MS [28]. ICP-TOF-MS is a near fully destructive technique that requires chemical dissolution of the sample[29], unlike RBS, which is non-destructive. Samples were taken from the collector probes by scraping off a region of the coating. It is critical in the analysis of each sample that repeated calibrations and comparisons with standards be performed to ensure that the system is clean before analysis and that there is no cross-contamination between samples in the system. The materials used for the probes (ATJ Graphite, Ted Pella Spectroscopically Pure Graphite) were tested in the ICP-TOF-MS to confirm that no significant levels of W were present in the original material that would interfere with the analysis of the deposited coatings.

The second ICP-MS technique used was Laser Ablation Inductively Coupled Plasma Mass Spectroscopy (LA-ICP-MS), which is appropriate for near surface rather than bulk sample analysis. The LA-ICP-MS system consisted of an Agilent 7700x [30] quadrupole ICP-MS combined with a NewWave UP-213nm Laser Ablation Tool. Instead of chemically dissolving a sample and injecting the liquid into the aerosolizer of the ICP-MS as is done for ICP-TOF-MS, a focused laser is used to ablate a region of a sample surface, and the liberated particulates are directed towards the plasma torch of the ICP-MS. Comparisons of measurements from the OTF side of the Type B probe inserted for the L-mode discharges described in the previous section using both ICP-TOF-MS and LA-ICP-MS are shown in subfigure a) of Figure 12 and demonstrate good agreement between the two techniques.

The W isotopic ratio measured on the collector probe is the result of the combination of the two sources of W in the divertor (isotopic fractions shown in Figure 11). A technique known as the Stable Isotope Mixing Model (SIMM) was used to analyze the coatings on the CPs.[31, 32] A full explanation of this method is beyond the scope of this paper and is the topic of another work; however, in short, the SIMM de-convolves the sources, and determines how much of the deposited material came from each source, thereby allowing the unique isotopic mixture on each CP to be traced back to its points of origin.

The SIMM begins with the isotopic fractions of each W isotope provided by ICP-MS, from which the W-182 isotopic fraction is shown in sub-figure a) of Figure 12. The result of the SIMM calculation is f, the relative fractional source from each of the two locations, shown in sub-figure b) of Figure 12. Going further, f is then combined with σ_W to form a fractional areal density from each source, as shown in sub-figure c) of Figure 12. For the specific case of the DIII-D MRC, f_{floor} is the natural W source located near the lower divertor pumping and f_{shelf} is the enriched W source from a location at the lower baffle region (see Figure 1). In this analysis, the SIMM assumes $f_{floor} + f_{shelf} = 1$.

The combined RBS, ICP-TOF-MS, and LA-ICP-MS analyses of the OTF side of the Type B probe from the repeated L-mode configuration (Shots 167196-167220) is shown in Figure 12 as a proof-of-principle case demonstrating the successful ability to identify the concentration of enriched W on the collector probe for a well-defined impurity source configuration. The position of the strike-points on the DIII-D divertor can be seen in Figure 1. The outer strike point was moved during the discharge from R = 1.60 m to the W-182 metal ring at R = 1.42 m, where it dwelled for 3.5 seconds, thereby avoiding any contact from the OSP with the natural W ring. A full triplet set of collector probes were held in place while this shot was repeated 25 times. The natural W source is located in a region of the divertor where there is very little particle flux expected for this magnetic configuration and therefore should not result in significant sputtering or contribution to the impurities in the system. These discharges took place at the beginning of the DIII-D MRC and were the first time the strike point was placed on either of the metal rings.

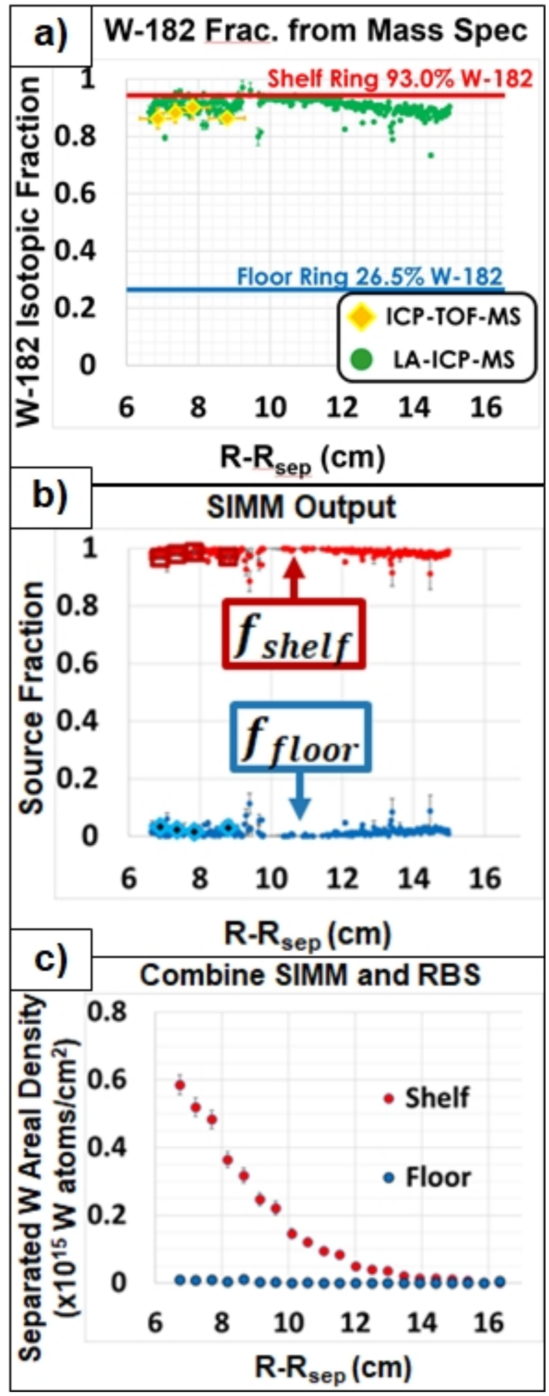

Figure 12: Analysis of the deposition profiles of the OTF side of the Type-B probe exposed for L-mode discharges 167196-167220. (a) Enrichment fraction of W-182 as measured by both ICP-TOF-MS (near the exposed tip) and LA-ICP-MS (along the full length). (b) Result of SIMM calculation. (c) SIMM fraction multiplied by the total W areal density as measured by RBS gives the W areal density on the probe from each divertor W source.

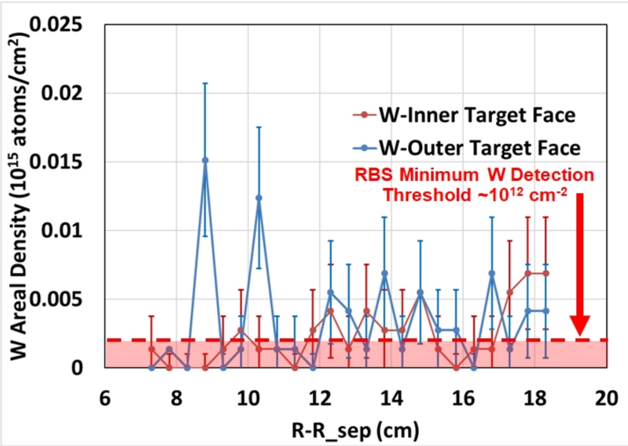

Figure 13: RBS survey of W areal density on collector probe exposed at the beginning of the DIII-D MRC to assess the background W content in the device before the plasma strikepoint was ever placed on the W inserts at the divertor.

Additional verification of this "clean" beginning was achieved by inserting a collector probe at the beginning of the DIII-D MRC (prior to these L-mode discharges) before any significant heat flux had been placed on either divertor W rings, which was then removed and analyzed with RBS (results shown in *Figure 13*). The W deposition along this CP was near the RBS measurement threshold and was on the order of 100 times lower than the content on the probes exposed during the L-mode discharges.

ICP-TOF-MS samples were taken in four locations over the 3 cm closest to the inner end of the probe and an axial scan was performed using LA-ICP-MS along the radial direction, as shown in sub-figure a) of Figure *12*. The results indicated that the average W-182 enrichment on the OTF side was 91.5% $\pm$ 2.6% for the exposed region from $R-R_{sep}$ = 6 to 12 cm. Entering these values into the SIMM along with the isotopic fraction of the other W isotopes to obtain the isotopic ratios, it was found that the contribution from the enriched W-182 metal ring was responsible for 99.3% $\pm$ 1.6% of the OTF deposition, indicating that nearly all of the W deposited on the collector probe came from the enriched W-182 ring. This was what was expected, of course, because the OSP was located on the enriched W-182 ring for all of the shots and the natural W ring was kept in region of negligible flux in the divertor where it should make little to no contribution to the influx of impurities in the system. These CP measurements represent a proof-of-principle experiment that verifies not only that sufficient amounts of W reached the far-SOL to be measured by RBS, but that isotopic distinction is also achievable and demonstrates that an enriched source is clearly distinguishable from the natural W signal that may come from any other source of W trace impurities in the system. Many additional CPs were exposed during discharges with the strike point on the natural W ring and the enriched W ring in the SOL resulting in more substantial source mixing, and discussion of those results with the associated physics interpretation are left to another work.

IV. Conclusions and Future Work

The above description of the analysis of the collector probes using RBS and ICP-MS to obtain elemental σ_W profiles highlighted the characteristic features of the collector probes and how they can be used to infer properties of impurity transport in the scrape-off layer. The truly novel contribution of this work is the combination of the collector probes with isotopic tracer particles, which allows a connection to be made between the source of impurities and the transport of the impurities in the scrape-off layer, thereby elucidating much more effectively aspects of the global impurity transport model than the collector probes alone could have provided.

There are three primary conclusions that have been identified from the use of collector probes during the DIII-D MRC. First, the σ_W deposition profiles measured on the CPs show the characteristics of typical CP profiles found in previous studies (exponential radially decaying profiles, re-erosion zone near the inner end). Second, a first-of-its-kind triplet probe has found asymmetries on the ITF/OTF sides of the probe with the longest sampling lengths (Type-A) but not on the probes with the shorter sampling lengths (Types B and C), providing never reported before data that is consistent with an upstream impurity potential well that has long been theorized as playing a fundamental role in edge impurity transport. Third, the viability of using enriched W isotopic tracer particles combined with the SIMM has been validated for the first time in an MFE experiment and provides a powerful new tool to relate impurity sources to impurity transport in the edge plasma. This has allowed the combination of the CPs with the isotopic tracer particles to become a global impurity transport diagnostic that paves the way for future uses to advance understanding of impurity transport in magnetically confined fusion.

The authors would like to acknowledge the contributions of the UT Institute for Nuclear Security for providing access to essential equipment and personnel. This work was supported by the US Department of Energy under DE-SC0016318 (UTK), DE-AC05-00OR22725 (ORNL), DE-FG02-07ER54917 (UCSD), DE-FC02-04ER54698 (General Atomics), DE-NA0003525 (SNL). DIII-D data shown in this paper can be obtained in digital format by following the links at https://fusion.gat.com/global/D3D_DMP. This report was prepared as an account of work sponsored by an agency of the United States Government. Neither the United States Government nor any agency thereof, nor any of their employees, makes any warranty, express or implied, or assumes any legal liability or responsibility for the accuracy, completeness, or usefulness of any information, apparatus, product, or process disclosed, or represents that its use would not infringe privately owned rights. Reference herein to any specific commercial

product, process, or service by trade name, trademark, manufacturer, or otherwise does not necessarily constitute or imply its endorsement, recommendation, or favoring by the United States Government or any agency thereof. The views and opinions of authors expressed herein do not necessarily state or reflect those of the United States Government or any agency thereof.

REFERENCES

[1]P. C. Stangeby Physics of Fluids **30,** (1987).
[2]S. A. Cohen Journal of Nuclear Materials **76-7,** (1978).
[3]D. Hildebrandt, H. Wolff, J. Roth, R. Brakel, P. Grigull, F. Rau, F. Sardei and E. Taglauer Journal of Nuclear Materials **196,** (1992).
[4]W. Schustereder, K. Krieger, A. Herrmann, V. Rohde and A. U. Team Journal of Nuclear Materials **363,** (2007).
[5]K. Krieger, et al. Journal of Nuclear Materials **241,** (1997).
[6]K. Krieger, H. Maier, R. Neu and A. U. Team Journal of Nuclear Materials **266,** (1999).
[7]P. Staib Journal of Nuclear Materials **111,** (1982).
[8]H. Grote Journal of Nuclear Materials **162,** (1989).
[9]J. P. Coad, D. E. Hole, M. Rubel, A. Widdowson, J. Vince and J.-E. Contributors Physica Scripta **T138,** (2009).
[10]K. Holtrop, D. Buchenauer, C. Chrobak, C. Murphy, R. Nygren, E. Unterberg and M. Zach Fusion Science and Technology**,** (2017).
[11]D. L. Rudakov, et al. Fusion Engineering and Design **124,** (2017).
[12]R. Neu, et al. Plasma Physics and Controlled Fusion **38,** (1996).
[13]R. Neu, et al. Plasma Physics and Controlled Fusion **44,** (2002).
[14]A. Geier, H. Maier, R. Neu, K. Krieger and A. U. Team Plasma Physics and Controlled Fusion **44,** (2002).
[15]C. P. C. Wong, et al. Journal of Nuclear Materials **363,** (2007).
[16]D. L. Rudakov, et al. Physica Scripta **T138,** (2009).
[17]Ted-Pella-Inc*,* edited by Ted-Pella-Inc (http://www.tedpella.com/carbon_html/carbon-rods-shapers.htm#anchor1279861, 2007).
[18]P. C. Stangeby, *The plasma boundary of magnetic fusion devices* (Institute of Physics Pub., Bristol ; Philadelphia, 2000).
[19]P. C. Stangeby and G. M. McCracken Nuclear Fusion **30,** (1990).
[20]W. R. Wampler, R. Bastasz, D. Buchenauer, D. Whyte, C. P. C. Wong, N. H. Brooks and W. P. West Journal of Nuclear Materials **233,** (1996).
[21]W. R. Wampler, P. C. Stangeby, J. G. Watkins, D. A. Buchenauer, D. L. Rudakov and C. P. C. Wong Journal of Nuclear Materials **438,** (2013).
[22]D. H. J. Goodall, W. O. Hofer, G. M. McCracken, R. Behrisch, M. Cowlin, K. J. Dietz, S. K. Erents and F. Thum Journal of Nuclear Materials **93-4,** (1980).
[23]D. Hildebrandt, H. Grote, A. Herrmann, M. Laux, P. Pech, H. D. Reiner and H. Wolff Contributions to Plasma Physics **28,** (1988).
[24]G. Staudenmaier, P. Staib and S. Rossnagel Journal of Nuclear Materials **111,** (1982).
[25]P. C. Stangeby and J. D. Elder Nuclear Fusion **35,** (1995).
[26]J. Neuhauser, W. Schneider, R. Wunderlich and K. Lackner Nuclear Fusion **24,** (1984).
[27]R. E. Sturgeon, J. W. H. Lam and A. Saint Journal of Analytical Atomic Spectrometry **15,** (2000).
[28]GBC-Scientific-Equipment*,* (GBC-Scientific-Equipment, http://www.gbcsci.com/products/icp-tof-ms/optimass-9500/).
[29]A. J. Bednar, W. T. Jones, M. A. Chappell, D. R. Johnson and D. B. Ringelberg Talanta **80,** (2010).
[30]S. Sannac, S. Takjiki and E. Moldenhauer, *Agilent Technologies, Inc.,* edited by I. Agilent Technologies (Agilent Technologies, Inc., 2013).
[31]J. G. Wiederhold Environmental Science & Technology **49,** (2015).
[32]D. L. Phillips Journal of Mammalogy **93,** (2012).